International Journal of Bifurcation and Chaos, Vol. 26, No. 5 (2016) 1650090 (13 pages)

DOI: 10.1142/S0218127416500905

Bifurcation and Spike Adding Transition in Chay–Keizer Model

Bo Lu*, Shenquan Liu†, Xuanliang Liu‡ and Xiaofang Jiang§
School of Mathematics,
South China University of Technology,
Guangzhou 510640, P. R. China
**cheersnow@163.com*
†*mashqliu@scut.edu.cn*
‡*liuliang@scut.edu.cn*
§*jiangxf5@yeah.net*

Xiaohui Wang
School of Mathematical and Statistical Sciences,
University of Texas-Rio Grande Valley,
Edinburg, TX 78539, USA
Xiaohui.wang@utrgv.edu

Received November 12, 2015

Electrical bursting is an activity which is universal in excitable cells such as neurons and various endocrine cells, and it encodes rich physiological information. As burst delay identifies that the signal integration has reached the threshold at which it can generate an action potential, the number of spikes in a burst may have essential physiological implications, and the transition of bursting in excitable cells is associated with the bifurcation phenomenon closely. In this paper, we focus on the transition of the spike count per burst of the pancreatic β-cells within a mathematical model and bifurcation phenomenon in the Chay–Keizer model, which is utilized to simulate the pancreatic β-cells. By the fast–slow dynamical bifurcation analysis and the bi-parameter bifurcation analysis, the local dynamics of the Chay–Keizer system around the Bogdanov–Takens bifurcation is illustrated. Then the variety of the number of spikes per burst is discussed by changing the settings of a single parameter and bi-parameter. Moreover, results on the number of spikes within a burst are summarized in ISIs (interspike intervals) sequence diagrams, maximum and minimum, and the number of spikes under bi-parameter value changes.

Keywords: Bogdanov–Takens bifurcation; spike adding; interspike intervals (ISIs); bursting, pancreatic β-cell; fast–slow dynamics analysis.

1. Introduction

The Chay–Keizer model, which was inspired by a hypothesis of Atwater and Rojas [Atwater *et al.*, 1980], was presented by Chay and Keizer [1983]. It is the original Hodgkin–Huxley type model for pancreatic β-cells, which are placed in cell clusters within the islets of Langerhans. The primary function of β-cells is tantamount to regulate glucose concentration in blood. Malfunctioning β-cells can cause type II diabetes [Lang *et al.*, 1981]. An important aspect of the Chay–Keizer model is to simulate and investigate the electrical activity of pancreatic

†Author for correspondence

β-cells. The model is used to understand the β-cell oscillations and insulin secretion [Pedersen, 2009; Félix-Martínez & Godínez-Fernández, 2014]. The kinetic properties of the model and some similar models such as the Wierschen–Bertram model [Yang & Guan, 2011] and the generic pituitary model [Tsaneva-Atanasova *et al.*, 2010] were studied [Bertram & Sherman, 2004; Zhang *et al.*, 2011; Teka *et al.*, 2011].

Various patterns of electrical activity can be observed in excitable cells such as neurons and different endocrine cells. The spiking and bursting electrical activity are ubiquitous in excitable cells, and there exist numerous known transition patterns between spiking and bursting such as a blue sky catastrophe [Shilnikov & Cymbalyuk, 2005], period doubling [Ye *et al.*, 2014], chaos [Medvedev, 2006], mixed-mode oscillations (MMOs) [Wojcik & Shilnikov, 2011] and so on. Dynamical mechanisms of these patterns have been investigated both experimentally and theoretically [Izhikevich, 2000; Koch & Segar, 1989; Terman, 1991; Desroches *et al.*, 2012]. Through use of mathematical models of neurons, besides studying the reasons for firing pattern generation, various dynamical properties associated with the process of firing pattern transitions have also been explored. For example, spiking adding mechanisms in transient bursts and the Hindmarsh–Rose burster have been tackled by using bifurcation analysis [Nowacki *et al.*, 2012; Linaro *et al.*, 2011].

The firing patterns of the single pancreatic β-cells also have their own characteristics. Two types of bursting oscillations have been prepared by using the technique of fast/slow analysis, plateau and pseudo-plateau bursting. Pseudo-plateau bursting, a type of canard-induced mixed-mode oscillation produced by some endocrine cells, is characterized by slight impulses or spikes which ride on top of a lift voltage plateau. It is different from plateau bursting, that is the standard classical square-wave bursting which often appears in neurons and many endocrine cells [Desroches *et al.*, 2013]. Given the functional significance of these types of bursting, it is important to comprehend the way in which they are organized and how they emerge and die. In addition, the number of spikes in a burst and differences in spike counts may have essential physiological implications. For instance, the number of spikes per burst may allow for discrimination among different types of certain stimulus features [Osinga & Tsaneva-Atanasova, 2010]. Mechanisms behind pseudo-plateau bursting generation in pituitary cells have been explicated [Vo *et al.*, 2010, 2014]. The switch from plateau to pseudo-plateau bursting has also been illustrated by using bifurcation analysis [Teka *et al.*, 2011]. However, altering the intra-burst spike count in pancreatic β-cells comes to nothing. So our study concerns the analysis of differences in the number of spikes within a burst based on the Chay–Keizer model.

The paper is organized as follows. In Sec. 2, bifurcation analysis for the Chay–Keizer model is presented through the fast–slow dynamical bifurcation theory [Yang & Lu, 2008] and the Bogdanov–Takens bifurcation theory [Carrillo *et al.*, 2010]. In Sec. 3, variations in the number of spikes within a burst are discussed and simulated by changing values of certain parameters. The rules behind the transition of the spike count are considered. Section 4 is a brief conclusion.

2. Model and Methodology

The Chay–Keizer model described the pancreatic islet electrical activities for the first time. The model has since been modified to produce subsequent models with similar structures. The basic model includes four types of currents, an inward Ca^{2+} current, I_{Ca}, an outward delayed rectifier K^+ current, I_K, a Ca^{2+}-dependent K^+ current, $I_{K(Ca)}$, and a ATP-sensitive K^+ current, $I_{K(ATP)}$. The differential equations for the membrane potential, V, activation of delayed rectifier K^+ channels, n, and cytosolic free Ca^{2+} concentration, c, are as follows:

$$\frac{dV}{dt} = -\frac{1}{C_m}[I_{Ca} + I_K + I_{K(Ca)} + I_{K(ATP)}], \quad (1)$$

$$\frac{dn}{dt} = \frac{n_\infty(V) - n}{\tau_n}, \quad (2)$$

$$\frac{dc}{dt} = f_{cyt} J_{mem}, \quad (3)$$

where C_m is the membrane capacitance, n_∞ denotes the steady state function for the gate variable n, τ_n represents the activation time constant for the delayed rectifier channel, f_{cyt} denotes the ratio of free to total Ca^{2+} in the cell, and J_{mem} represents the flux of Ca^{2+} through the plasma membrane. Expressions for the ionic currents are governed by

$$I_{Ca} = g_{Ca} m_\infty(V)(V - V_{Ca}),$$

$$I_K = g_K n(V - V_K),$$

$$I_{\mathrm{K(Ca)}} = g_{\mathrm{K(Ca)}} s_\infty(c)(V - V_{\mathrm{K}}),$$

$$I_{\mathrm{K(ATP)}} = g_{\mathrm{K(ATP)}}(V - V_{\mathrm{K}}),$$

where parameters V_{Ca} and V_{K} are the reversal potentials for Ca^{2+} and K^+ respectively. Parameters $g_{\mathrm{Ca}}, g_{\mathrm{K}}, g_{\mathrm{K(Ca)}}$ and $g_{\mathrm{K(ATP)}}$ are the maximal conductance for the various types of channels. Here m_∞ denotes the steady state activation function for the inward Ca^{2+} current, and s_∞ shows the fraction of K(Ca) channels activated by cytosolic Ca^{2+}. Expressions of these steady state activation functions are described by

$$m_\infty(V) = \left(1 + \exp\left(\frac{v_m - V}{s_m}\right)\right)^{-1},$$

$$n_\infty(V) = \left(1 + \exp\left(\frac{v_n - V}{s_n}\right)\right)^{-1},$$

$$s_\infty(c) = \frac{c^5}{c^5 + K_d^5},$$

where parameters v_m and v_n are the values of voltage when m_∞ and n_∞ reach their half-maximum values. Parameters s_m and s_n show the slopes of the m_∞ and n_∞ curves, respectively. In addition, parameter K_d denotes the dissociation constant for Ca^{2+} binding to the K(Ca) channel. Finally, the Ca^{2+} flux through the membrane is

$$J_{\mathrm{mem}} = -(\alpha I_{\mathrm{Ca}} + k_{\mathrm{PMCA}} c),$$

where α transforms units of current to units of flux, and k_{PMCA} denotes the rate of Ca^{2+} expulsion from the cell, i.e. the pump rate. Values of parameters used in the above model are listed as follows: $C_m = 5300\,\mathrm{fF}$, $g_{\mathrm{Ca}} = 1200\,\mathrm{pS}$, $g_{\mathrm{K}} = 6000\,\mathrm{pS}$, $g_{\mathrm{K(Ca)}} = 700\,\mathrm{pS}$, $g_{\mathrm{K(ATP)}} = 230\,\mathrm{pS}$, $v_m = -20\,\mathrm{mV}$, $v_n = -16\,\mathrm{mV}$, $V_{\mathrm{Ca}} = 25\,\mathrm{mV}$, $V_{\mathrm{K}} = -75\,\mathrm{mV}$, $s_m = 12\,\mathrm{mV}$, $s_n = 5\,\mathrm{mV}$, $\tau_n = 16\,\mathrm{ms}$, $K_d = 0.3\,\mu\mathrm{M}$, $\alpha = 4.5 \times 10^{-6}\,\mathrm{fA}^{-1}\mu\mathrm{Mms}^{-1}$, $k_{\mathrm{PMCA}} = 0.2\,\mathrm{ms}^{-1}$, and $f_{\mathrm{cyt}} = 0.01$.

The model was simulated in Python and Matcont, and all charts were also plotted using mathematical softwares.

3. Main Results

3.1. *Bifurcation analysis of equilibria of Chay–Keizer model*

Mixed-mode oscillations such as plateau bursting and pseudo-plateau busting were observed in the numerical simulation, and similar bursting was also found and studied in many neurons and endocrine cells [Vo *et al.*, 2010, 2014; Teka *et al.*, 2011]. Utilizing geometric singular perturbation, the mixed-mode oscillations of generation mechanism of the endocrine pituitary was revealed [Vo *et al.*, 2010, 2014]. The fast–slow dynamical bifurcation analysis [Izhikevich, 2000] can also be used to study the transition of firing patterns. Different types of bursting in neurons and endocrine cells were studied [Yang & Lu, 2008; Meng *et al.*, 2011; Lu *et al.*, 2004]. Therefore, in this part we are going to investigate the transition of plateau bursting and pseudo-plateau busting in pancreatic β-cells.

Various types of firing patterns are shown in Fig. 1. The first two figures present square-wave bursting, i.e. plateau bursting. Figure 1(d) shows the triangular type of bursting and the pseudo-plateau busting appears as the parameter f_{cyt} increases. They all belong to mixed-mode oscillations, and can be found in psychological experiments [Kinard *et al.*, 1999].

Because f_{cyt} is usually a small quantity and then c varies much slower than other variables, the system (1)–(3) is a multi-timescale problem for which there are two fast and one slow variables in the model. We can use the fast/slow dynamics analysis to study the transition of firing patterns. A fast subsystem is governed by

$$\frac{dV}{dt} = -\frac{1}{C_m}[I_{\mathrm{Ca}} + I_{\mathrm{K}} + I_{\mathrm{K(Ca)}} + I_{\mathrm{K(ATP)}}], \quad (4)$$

$$\frac{dn}{dt} = \frac{n_\infty(V) - n}{\tau_n}. \quad (5)$$

Equilibria for the fast subsystem is given by the following equations:

$$I_{\mathrm{Ca}} + I_{\mathrm{K}} + I_{\mathrm{K(Ca)}} + I_{\mathrm{K(ATP)}} = 0, \quad (6)$$

$$\frac{n_\infty(V) - n}{\tau_n} = 0. \quad (7)$$

The nullcline of the slow variable c satisfies the following condition:

$$c = -\frac{\alpha g_{\mathrm{Ca}} m_\infty(V)(V - V_{\mathrm{Ca}})}{k_{\mathrm{PMCA}}}.$$

When the slow variable c is taken as the bifurcation parameter of the fast subsystem, a Z-shaped bifurcation curve of the equilibrium points of the fast subsystem (4)–(5) in the (c, V)-phase plane

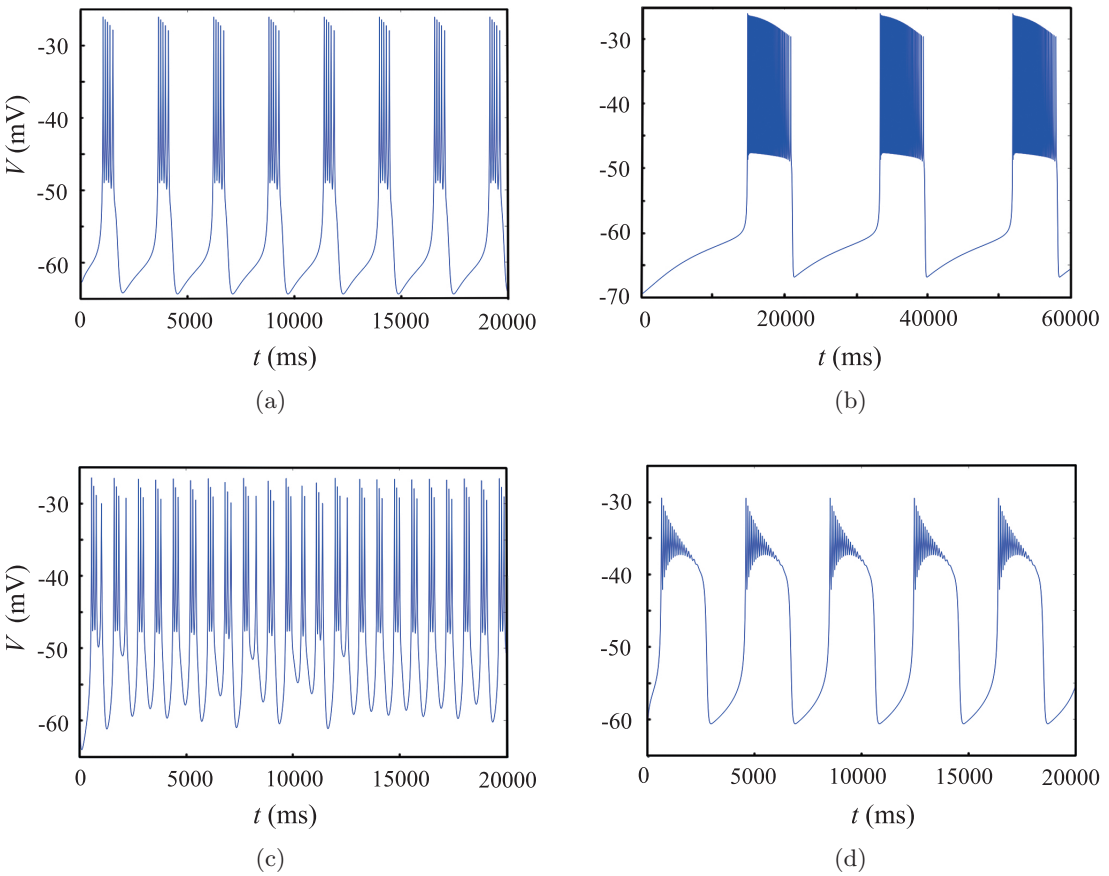

Fig. 1. Diverse types of time course of membrane potential with different values of parameters. (a) The low frequency square-wave bursting at $V_K = -75$ and $f_{cyt} = 0.006$, (b) the high frequency square-wave bursting at $V_K = -75$ and $f_{cyt} = 0.0005$, (c) the time course in the chaotic region at $V_K = -73$ and $f_{cyt} = 0.006$ and (d) the tapered bursting at $V_K = -70$ and $f_{cyt} = 0.0005$.

for $V_K = -73\,\text{mV}$ and $f_{cyt} = 0.0001$ is displayed in Fig. 2(a), and the trajectory of the bursting is superimposed on the bifurcation curve. Two Hopf bifurcation points (H_1 and H_2) occur on the upper branch of the Z-shaped bifurcation curve, where the stable focus of the fast subsystem loses its stability via the Hopf bifurcation at H_1 (at $c = -0.203366$), and the stable limit cycle, depicted with the maximum and minimum values of the membrane potential V (the solid curves), arises around the unstable focus and then disappears and returns to the stable focus via the Hopf bifurcation at H_2 (at $c = 0.203923$). The middle and lower branches of the Z-shaped bifurcation curve are composed of saddles (the dashed curve) and stable nodes (the solid curve), respectively. The rest state on the lower branch of the Z-shaped bifurcation curve vanishes and transits to the spiking state corresponding to the stable limit cycle around the upper branch of the bifurcation curve via the fold bifurcation at LP_1. And the upper rest state transits to the lower rest state via the fold bifurcation at LP_2. Moreover, besides the above two bifurcations which result in the emergence and termination of the spike state, the bifurcations of hysteresis loop are also considered. Thus, the bursting whose shape is tapered displays dynamical behavior of the fold/Hopf bursting via the fold/fold hysteresis loop, and the pseudo-plateau busting appears as the parameter f_{cyt} increases.

As the reversal potential of the potassium ion decreases, the Hopf point H_1 closes into LP_2 and the saddle homoclinic bifurcation occurs at $V_K = -75$ in Fig. 2(c). Then the spiking state returns to the rest state via the saddle homoclinic bifurcation which is different from the above case. Thus the bursting whose shape is square-wave displays dynamical behavior of the fold/homoclinic bursting via the fold/homoclinic hysteresis loop. The number of spikes per burst decreases as the parameter f_{cyt} increases. The change of distance between H_1 and LP_2 can be clearly observed in Fig. 2(d).

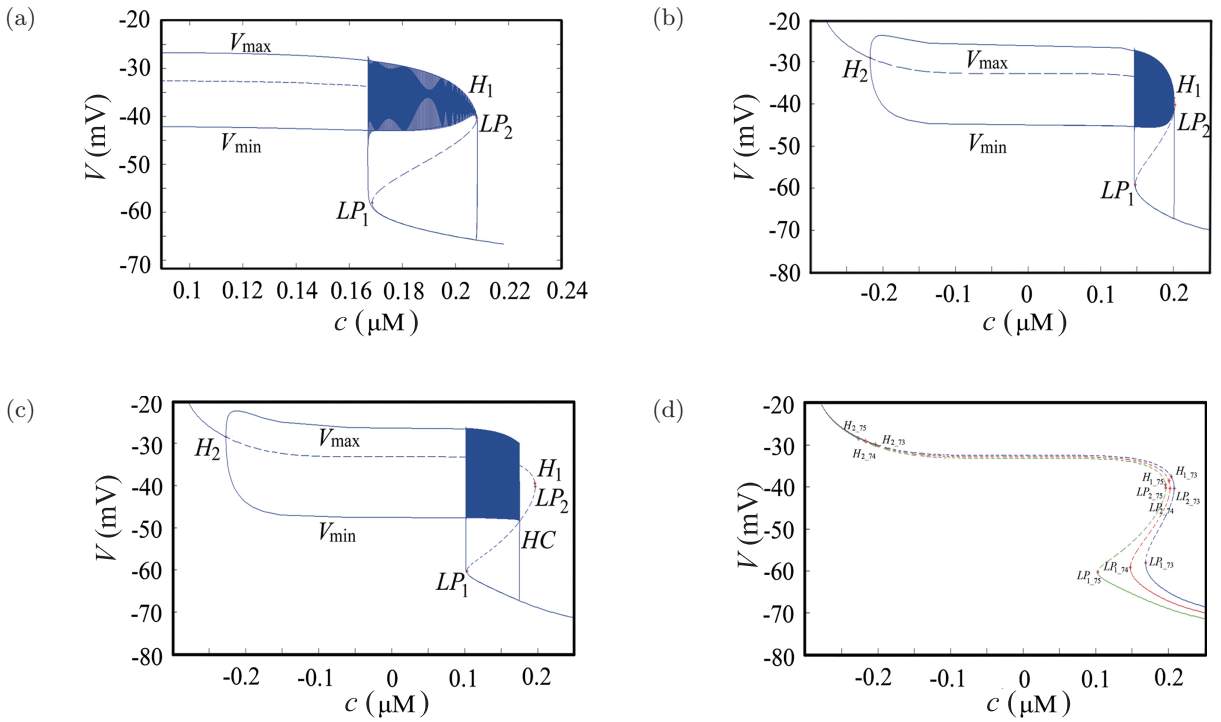

Fig. 2. The fast–slow dynamic bifurcation analysis. (a)–(c) Bifurcation diagrams of equilibria for the fast subsystem with respect to the slow variable c for $V_K = -73\,\text{mV}$, $V_K = -74\,\text{mV}$ and $V_K = -75\,\text{mV}$, respectively. The corresponding phase portraits of all systems are superimposed on the bifurcation curves. Here H_1 and H_2 represent the subcritical Hopf bifurcation points, LP_1 and LP_2 represent the fold bifurcation points, and V_{max} and V_{min} represent the maximum and minimum values of the membrane potential V, respectively. (d) Bifurcation of equilibria for the fast subsystem for different values of V_K ($V_K = -73\,\text{mV}$ (blue), $V_K = -74\,\text{mV}$ (red), $V_K = -75\,\text{mV}$ (green)), where H_{1_x} and H_{2_x} represent the subcritical Hopf bifurcation points at $V_K = -x\,\text{mV}$, and LP_{1_x} and LP_{2_x} represent the fold bifurcation points at $V_K = -x\,\text{mV}$ with $x = 73, 74, 75$, respectively.

The reversal potential of the potassium ion V_K and the ratio of free to total Ca^{2+} in the cell f_{cyt} affect the firing patterns of the pancreatic β-cells which are governed by the Chay–Keizer model. Hence, these parameters related to the channels of the potassium ion and the calcium ion are considered to explore the spike adding transition in the pancreatic β-cells. Furthermore, codimension-2 bifurcations of equilibria are considered in the section. We first present a bifurcation diagram for the Chay–Keizer model (1)–(3) in the (V_K, f_{cyt}) two-dimensional parameter space. Then, the Bogdanov–Takens bifurcation is investigated by combining the bifurcation theory of ordinary differential equations and the numerical simulations.

Figure 3 shows the bi-parameter bifurcation diagram of the Chay–Keizer model. The abscissa and the ordinate are V_K and f_{cyt}, respectively. The red curves denote the saddle-node bifurcation curves SN_1 and SN_2, and the blue curve is the Hopf bifurcation curve denoted by H in Fig. 3. The codimension-2 Bogdanov–Takens bifurcation BT_1 and BT_2 are placed on the saddle-node bifurcation curves SN_1 and SN_2. Then the types of bifurcations of equilibria in the Chay–Keizer model (1)–(3) near the Bogdanov–Takens bifurcation are investigated by Carrillo *et al.* [2010].

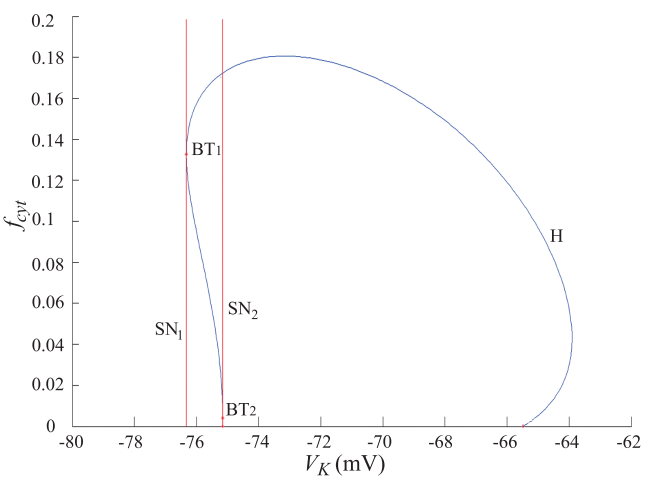

Fig. 3. Two-parameter bifurcation diagram in the (V_K, f_{cyt})-plane. All parameters are as indicated in Sec. 2.

$(V_{\rm K}, f_{\rm cyt})$ is taken as bifurcation parameters in the system (1)–(3). The Bogdanov–Takens bifurcation point $\rm BT_1$ appears at $(V_{\rm K}, f_{\rm cyt}) = (-76.323729, 0.132641) \triangleq \mu_0$ in Fig. 2, and the coordinate of the corresponding equilibrium point is $(V, n, c) = (-51.202700, 0.000875, 0.142221) \triangleq X_0$. The system (1)–(3) can be rewritten in the following form:

$$\frac{dX}{dt} = F(X, \mu), \tag{8}$$

where $X = (V, n, c)^T$, $\mu = (V_{\rm K}, f_{\rm cyt})^T$, and

$$F(X,\mu) = \begin{pmatrix} -\dfrac{1}{C_m}[g_{\rm Ca} m_\infty(V)(V - V_{\rm Ca}) + g_{\rm K} n(V - V_{\rm K}) + g_{\rm K(Ca)} s_\infty(c)(V - V_{\rm K}) + g_{\rm K(ATP)}(V - V_{\rm K})] \\ \dfrac{n_\infty(V) - n}{\tau_n} \\ -f_{\rm cyt}(\alpha g_{\rm Ca} m_\infty(V)(V - V_{\rm Ca}) + k_{\rm PMCA} c) \end{pmatrix}.$$

The Taylor expansion of $F(X, \mu)$ around (X_0, μ_0) is

$$F(X,\mu) = DF(X_0,\mu_0)(X - X_0) + F_\mu(X_0,\mu_0)(\mu - \mu_0) + \frac{1}{2} D^2 F(X_0,\mu_0)(X - X_0, X - X_0) + F_{\mu X}(X_0,\mu_0)(\mu - \mu_0, X - X_0) + \cdots,$$

where

$$A \triangleq \begin{pmatrix} 0.02938950305 & -28.43890076 & -2.663944021 \\ 0.00001092652569 & -0.0625 & 0 \\ 0.0002431610798 & 0 & -0.0265282 \end{pmatrix}.$$

The eigenvalues of matrix A are 0, 0, and -0.05963869695, respectively.

Let $P = (p_1, p_2, p_0)$ and P is an invertible matrix. We change matrix A into the Jordan normal form. That is

$$P^{-1} A P = \begin{pmatrix} 0 & 1 & 0 \\ 0 & 0 & 0 \\ 0 & 0 & -0.05963869695 \end{pmatrix},$$

with

$$J_0 = \begin{pmatrix} 0 & 1 \\ 0 & 0 \end{pmatrix}, \quad J_1 = -0.05963869695.$$

Then we have

$$p_1 = (1, 0.0001748269236, 0.009166267388)^T, \quad p_2 = (1, -0.002622406367, -0.3363630517)^T,$$
$$p_0 = (261.8675992, 1, -1.923136590)^T.$$

Let $P^{-1} = (q_1, q_2, q_0^T)^T$. Then we get

$$q_1 = (0.9988356930, -252.0724804, 4.934763681)^T,$$
$$q_2 = (0.02780095068, -12.64900851, -2.791710339)^T,$$
$$q_0 = (-0.0001017179813, 1.010898216, -0.008183728522).$$

By a straightforward calculation as described in [Carrillo *et al.*, 2010], we obtain

$$\begin{aligned}
a &= \frac{1}{2}p_1^T(q_2 \cdot D^2F(X_0,\mu_0))p_1 = -0.00008872816565,\\
b &= p_1^T(q_1 \cdot D^2F(X_0,\mu_0))p_1 + p_1^T(q_2 \cdot D^2F(X_0,\mu_0))p_2 = 0.00261000317,\\
S_1 &= F_\mu^T(X_0,\mu_0)q_2 = (0.001319860312, 2.034877666\times 10^{-7})^T,\\
S_2 &= \left[\frac{2a}{b}(p_1^T(q_1 \cdot D^2F(X_0,\mu_0))p_2 + p_2^T(q_2 \cdot D^2F(X_0,\mu_0))p_2) - p_1^T(q_2 \cdot D^2F(X_0,\mu_0))p_2\right] F_\mu^T(X_0,\mu_0)q_1\\
&\quad - \frac{2a}{b}\sum_{i=1}^{2}(q_i \cdot (F_{\mu X}(X_0,\mu_0) - ((p_0J_1^{-1}q_0)F_\mu(X_0,\mu_0))^T \times D^2F(X_0,\mu_0)))p_i\\
&\quad + (q_2 \cdot (F_{\mu X}(X_0,\mu_0) - ((p_0J_1^{-1}q_0)F_\mu(X_0,\mu_0))^T D^2F(X_0,\mu_0)))p_1\\
&= (-0.0450512112, -0.01078127854)^T.
\end{aligned}$$

Note that $\lambda_1 = V_{\rm K} + 76.323729$ and $\lambda_2 = f_{\rm cyt} - 0.132641$. It gives

$$\begin{aligned}
\beta_1 &= S_1^T(\mu-\mu_0) = 0.001319860312\lambda_1\\
&\quad + 2.034877666\times 10^{-7}\lambda_2,\\
\beta_2 &= S_2^T(\mu-\mu_0) = -0.0450512112\lambda_1\\
&\quad - 0.01078127854\lambda_2.
\end{aligned}$$

According to [Carrillo *et al.*, 2010], we know the dynamics on the center manifold of system (1)–(3) is locally topologically equivalent to the following system at the Bogdanov–Takens bifurcation (X_0,μ_0):

$$\begin{cases}
\dot z_1 = z_2,\\
\dot z_2 = \beta_1 + \beta_2 z_1 + az_1^2 + bz_1z_2\\
\quad = 0.001319860312\lambda_1 + 2.034877666\times 10^{-7}\lambda_2\\
\quad\quad - (0.0450512112\lambda_1 + 0.01078127854\lambda_2)z_1\\
\quad\quad - 0.00008872816565z_1^2 + 0.00261000317z_1z_2.
\end{cases} \tag{9}$$

Furthermore, by virtue of the transformations

$$\begin{aligned}
t &= \frac{0.00261000317}{0.00008872816565}t_1,\\
z_1 &= \frac{0.00008872816565}{(0.00261000317)^2}\eta_1,\\
z_2 &= -\frac{(0.00008872816565)^2}{(0.00261000317)^3}\eta_2
\end{aligned}$$

the system (9) can be changed to

$$\begin{cases}
\dfrac{d\eta_1}{dt_1} = \eta_2,\\
\dfrac{d\eta_2}{dt_1} = \overline{\beta}_1 + \overline{\beta}_2\eta_1 + \eta_1^2 - \eta_1\eta_2,
\end{cases} \tag{10}$$

where

$$\overline{\beta}_1 = -0.08768142511\lambda_1 - 0.00001351817098\lambda_2$$

and

$$\overline{\beta}_2 = -38.98212725\lambda_1 - 9.328876202\lambda_2.$$

Applying the theory of the Bogdanov–Takens bifurcation [Kuznetsov, 1998], we obtain

Theorem 1. *Let* $\lambda_1 = V_{\rm K} + 76.323729$ *and* $\lambda_2 = f_{\rm cyt} - 0.132641$. *If the values of parameters* ($V_{\rm K}$, $f_{\rm cyt}$) *change around* $(-76.323729, 0.132641)$, *and other parameters in system (1)–(3) are indicated as in Sec. 2, then system (1)–(3) is locally topologically equivalent to the following system at the Bogdanov–Takens bifurcation* BT_1:

$$\begin{cases}
\dfrac{d\eta_1}{dt_1} = \eta_2,\\
\dfrac{d\eta_2}{dt_1} = -0.08768142511\lambda_1 - 0.00001351817098\lambda_2\\
\quad\quad - (38.98212725\lambda_1 + 9.328876202\lambda_2)\eta_1\\
\quad\quad + \eta_1^2 - \eta_1\eta_2,
\end{cases} \tag{11}$$

which has the following local bifurcation behaviors in a small neighborhood of the origin.

(i) *There is a saddle-node bifurcation curve*

$$SN = \{(\lambda_1, \lambda_2) : \lambda_1^2 + 0.4786232491\lambda_1\lambda_2 + 0.05727005366\lambda_2^2 + 0.0002308003811\lambda_1 + 3.558352 \times 10^{-8}\lambda_2 = 0\}.$$

(ii) *There is an Andronov–Hopf bifurcation curve*

$$H = \{(\lambda_1, \lambda_2) : \lambda_1 = -0.0001541737143\lambda_2, \lambda_1 + 0.2393116249\lambda_2 > 0\}.$$

(iii) *There is a homoclinic bifurcation curve*

$$HL = \{(\lambda_1, \lambda_2) : \lambda_1^2 + 0.4786232492\lambda_1\lambda_2 + 0.05727005368\lambda_2^2 - 0.0002404170637\lambda_1 - 3.706599168 \times 10^{-8}\lambda_2 = o(|\lambda_1, \lambda_2|^2), \lambda_1 + 0.2393116249\lambda_2 > 0\}.$$

The bifurcation behavior in a small neighborhood of the origin at the Bogdanov–Takens bifurcation BT_2 can also be computed in a similar manner.

3.2. *Influence of single parameters on spike adding*

Spike adding, that the system alters its behavior from spiking to bursting with increasing number of spikes per bursts by changing a parameter, arises in many neurons and endocrine cells [Nowacki *et al.*, 2012; Linaro *et al.*, 2011]. This phenomenon in pancreatic β-cells has been observed [Teka *et al.*, 2011] experimentally, and in the Chay–Keizer model, by changing the parameter v_n and f_{cyt} it can also be observed. In addition, other alterations of parameters such as V_K, g_K, and so on, lead to similar results. In this section we attempt to change the values of V_K to explore spike adding in the Chay–Keizer model.

The sequences of the action potential interspike intervals (ISIs) are used to describe the transition of spike adding phenomenon in the Chay–Keizer model, and ISIs can be given as the following derivation process.

Suppose that the periodic solution $V(t)$ of system (1)–(3) reaches the first maximum, the first minimum and the adjacent maximum at time t_1, t_2 and t_3, respectively. We rewrite Eq. (1) in the form

$$\frac{C_m dV}{-[I_{\text{Ca}} + I_{\text{K}} + I_{\text{K(Ca)}} + I_{\text{K(ATP)}}]} = dt. \quad (12)$$

We notice that the left-hand side of Eq. (12) has different expression in two time intervals $[t_1, t_2]$ and $[t_2, t_3]$. Thus, we let

$$\frac{C_m}{-[I_{\text{Ca}} + I_{\text{K}} + I_{\text{K(Ca)}} + I_{\text{K(ATP)}}]} \triangleq \begin{cases} F_1(V), & \text{if } t \in [t_1, t_2], \\ F_2(V), & \text{if } t \in [t_2, t_3]. \end{cases}$$

The decreasing period of time of $V(t)$ can be expressed as

$$\int_{V_{\max}}^{V_{\min}} F_1(V)dV = \int_{t_1}^{t_2} dt \triangleq T_{\text{down}}$$

and the increasing period of time of $V(t)$ is

$$\int_{V_{\min}}^{V_{\max}} F_2(V)dV = \int_{t_2}^{t_3} dt \triangleq T_{\text{up}},$$

where $V_{\min}$ and $V_{\max}$ denote the minimum and maximum of $V(t)$, respectively.

So, the expression of ISIs can be given by integro-differential equations (1)–(3) and the following equation

$$\text{ISIs} = T_{\text{down}} + T_{\text{up}} = \int_{V_{\max}}^{V_{\min}} F_1(V)dV + \int_{V_{\min}}^{V_{\max}} F_2(V)dV. \quad (13)$$

Then the bifurcation phenomenon of ISIs can be observed through numerical simulations.

As Fig. 4 shows, with $f_{\text{cyt}} = 0.0005$ and all other parameter sets to be default values, the

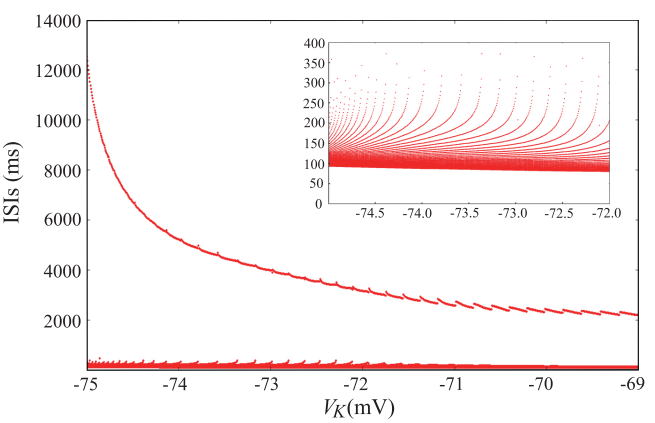

Fig. 4. The bifurcation diagram of ISIs without chaos. The subgraph is the amplified image for $-75 < V_K < -72$.

sequences of the action potential ISIs show a clear period adding bifurcation phenomenon with the perturbation of the reversal potential of the potassium ion. By observing the time course of action potentials it can be found that the conical bursting appears at $V_{\mathrm{K}} = -69$ and there are 12 spikes per burst. When the value of V_{K} approximates -71.5, the shape of the bursts transforms to a square. Finally, the Chay–Keizer model develops a plateau bursting pattern, and the endocrine cell achieves resting when $V_{\mathrm{K}} < -75.15$. Moreover, the number of spikes per burst increases without chaos continuously throughout the whole process.

However, when we take the value of $f_{\mathrm{cyt}} = 0.006$, period doubling bifurcation with chaos in the sequences of the action potential ISIs appears.

Then, the maximum and minimum of the action potential is also considered to examine spike adding in the Chay–Keizer model. Extremes of periodic solution $V(t)$ should satisfy the algebraic differential equations (1)–(3) and (6). That is

$$\begin{cases} \dfrac{dV}{dt} = -\dfrac{1}{C_m}[I_{\mathrm{Ca}} + I_{\mathrm{K}} + I_{\mathrm{K(Ca)}} + I_{\mathrm{K(ATP)}}], \\ \dfrac{dn}{dt} = \dfrac{n_\infty(V) - n}{\tau_n}, \\ \dfrac{dc}{dt} = -f_{\mathrm{cyt}}(\alpha g_{\mathrm{Ca}} m_\infty(V)(V - V_{\mathrm{Ca}}) + k_{\mathrm{PMCA}} c), \\ I_{\mathrm{Ca}} + I_{\mathrm{K}} + I_{\mathrm{K(Ca)}} + I_{\mathrm{K(ATP)}} = 0. \end{cases}$$

The bifurcation of extremes can also be presented by numerical simulations. It means that the pitchfork bifurcation may occur in algebraic differential equations (1)–(3) and (6).

Based on the Chay–Keizer model, the endocrine cell begins to generate spiking at approximately $V_{\mathrm{K}} = -64.5$. While the parameter V_{K} decreases, the amplitude of spikes magnifies continuously. Moreover, this can be proved by the changes of the spikes' maximum and minimum values as illustrated in Fig. 6. And then bursting arises from $V_{\mathrm{K}} = -66.232$, and there are two spikes in a burst at that moment. The period doubling bifurcation of the sequences of the action potential ISIs can be observed clearly in Figs. 5(a) and 6. With the increasing of the period doubling bifurcation, a chaotic region is formed when the value of V_{K} is taken between -68.9 and -68.27. In addition, the largest Lyapunov exponent of the system (1)–(3) is positive at this interval in Fig. 5(b). After this region, new bursting which has three spikes per burst can be obtained. With continued decreasing of the parameter V_{K}, the other chaotic region is created at $-73.18 < V_{\mathrm{K}} < -72.64$. Then passing through this chaotic region, bursting with four or more spikes per burst arises. Finally, the cell enters a resting state at $V_{\mathrm{K}} < -75.156$.

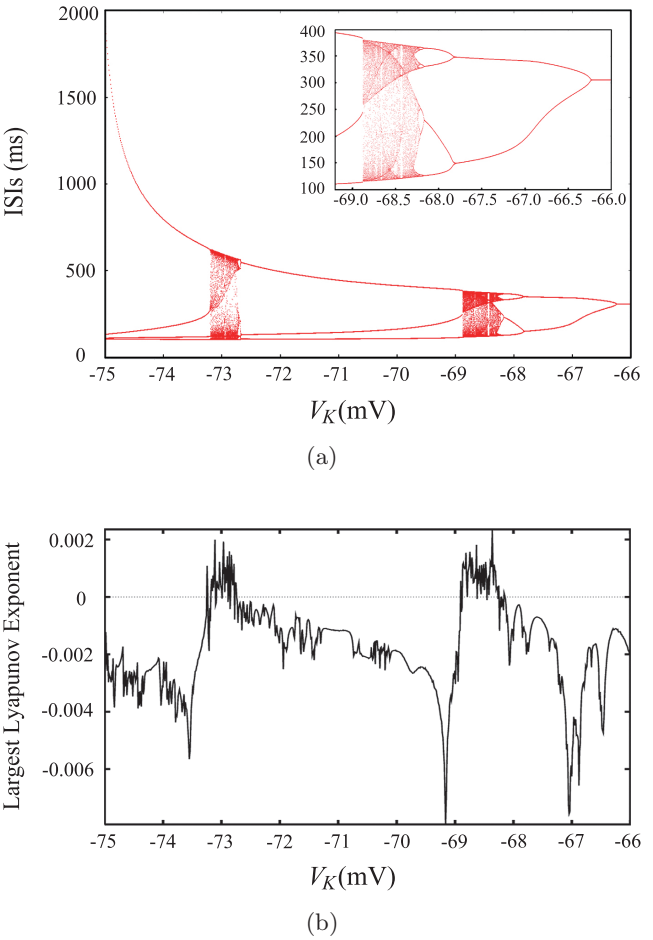

Fig. 5. (a) The bifurcation diagram of ISIs with chaos and the subgraph is the amplified image for $-69.2 < V_{\mathrm{K}} < -66$ and (b) the variety of the largest Lyapunov exponent with V_{K}.

Differences in the number of spikes per burst can also be illustrated by the maximum and minimum of the action potential. From Fig. 6 we can see that, when $V_{\mathrm{K}} > -65$, there is a single line in the graph. It means that the cells maintain quiescence. Then the spiking pattern arises in cells when the period doubling bifurcation of the sequences of the maximum and minimum of action potential occurs at $V_{\mathrm{K}} = -65$. The period doubling bifurcation goes on occurring, so the firing patterns transform from spiking into the bursting. In addition, the number of

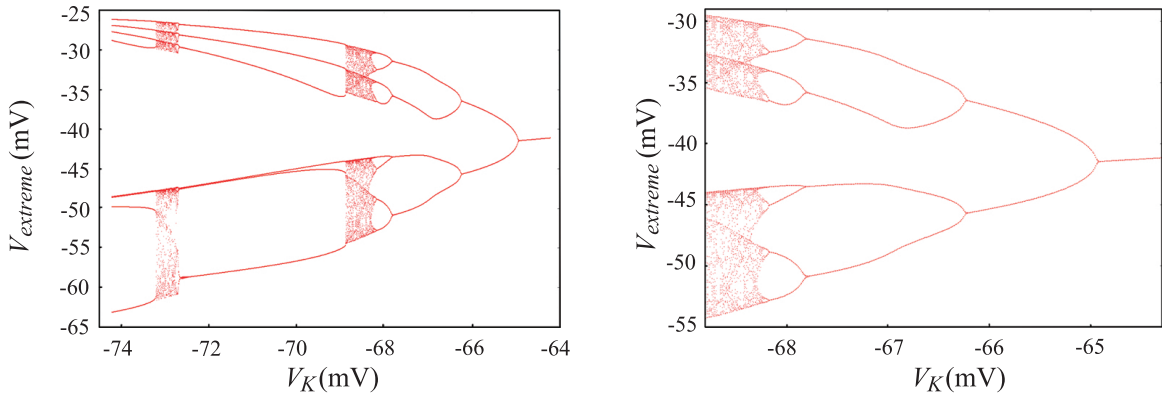

Fig. 6. The bifurcation diagram of extremes for spikes without chaos. The subgraph (b) is an amplified image of (a) from $-69 < V_{\mathrm{K}} < -64$.

spikes within a burst keeps on increasing throughout the chaotic region.

The number of spikes per burst can be transformed by changing the values of other parameters. For example, the bifurcation of ISIs with chaos and without chaos can occur with changing values of f_{cyt}. Furthermore, the period doubling bifurcation and the inverse period doubling bifurcation of the ISIs are also observed when the value of v_n is changed, which can also give rise to the chaotic regions and can cause the spike adding phenomenon as shown in Figs. 7 and 8.

3.3. *Influence of bi-parameter on spike adding*

In the above context, we mainly study the effect of one parameter on spike adding in pancreatic β-cells which are governed by the Chay–Keizer model. In particular, the influence which is caused by V_{K} to the variety of the spike counts which appear for a single burst is explored. Moreover, the spike adding phenomenon is also observed when the values of other parameters are changed, such as f_{cyt}, g_{K}, and so on. Due to this, we consider spike adding to be affected by modifications of the values of two parameters simultaneously. Based on the study above, besides the parameter V_{K}, we take the parameter f_{cyt} in the slow subsystem (3) and consider the regular pattern of change in the number of spikes per burst.

In Sec. 3.2, we know that, with $f_{\mathrm{cyt}} = 0.0005$ the system (1)–(3) can generate the period adding bifurcation phenomenon without chaotic regions, and the firing patterns are plateau and pseudo-plateau bursting. Thus, the range of parameter f_{cyt} is taken as 0.0005–0.0003 to study the spike count.

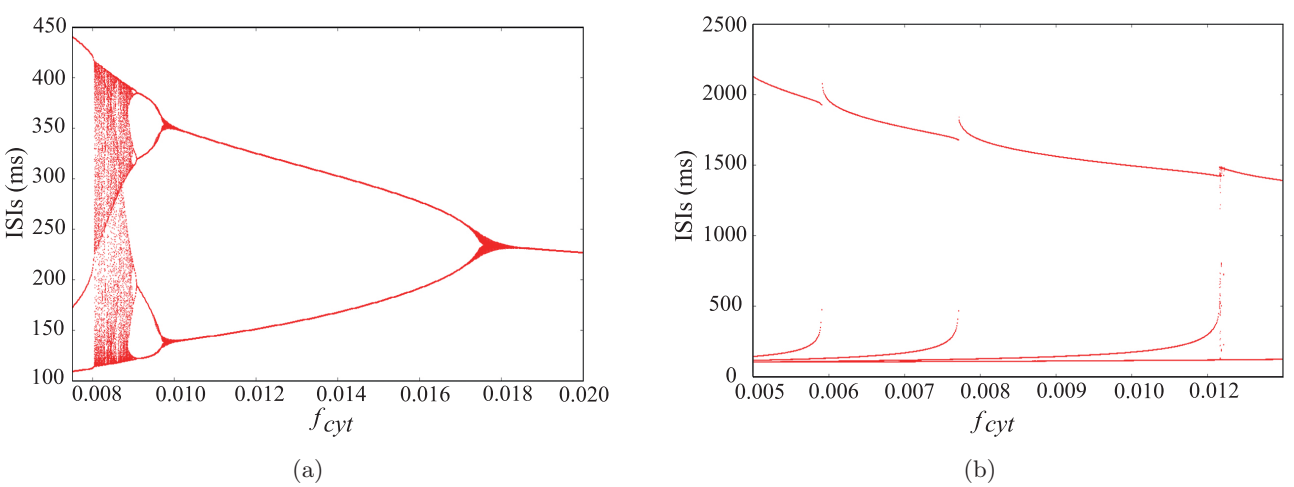

Fig. 7. The period doubling and period adding bifurcation diagram of f_{cyt} versus ISIs. Subgraphs are illustrations of partial enlargement, respectively.

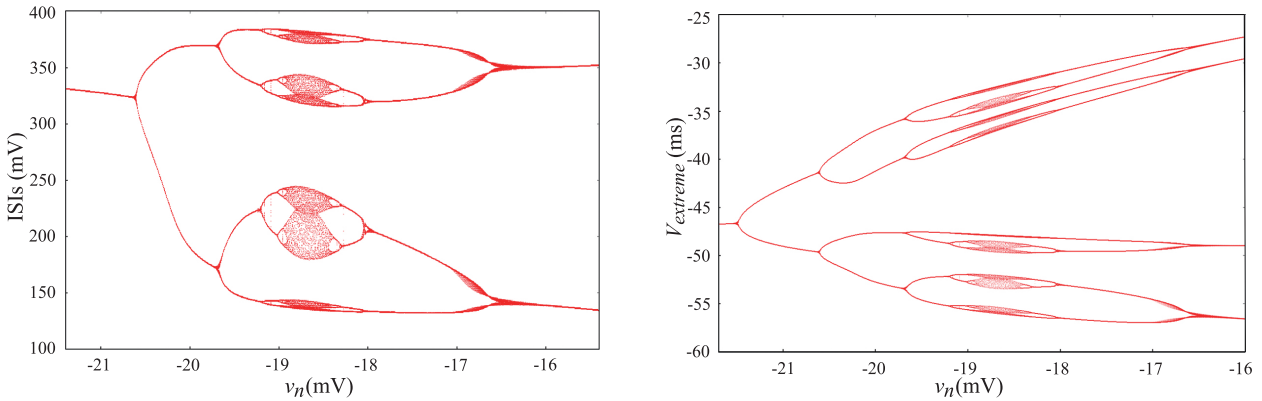

(a) (b)

Fig. 8. (a) The period doubling bifurcation and the inverse period doubling bifurcation diagram of the ISIs with changing values of parameter v_n and (b) the period doubling bifurcation and the inverse period doubling bifurcation diagram of the maximum and minimum.

In Fig. 9, the abscissa denotes the parameter V_{K} whose value is taken from -75 to -69, and the ordinate is the parameter f_{cyt} whose value is taken from 0.0005 to 0.003. In addition, colorful belt areas in the plane indicate the number of spikes in a burst. Observing this diagram, we can discover that the number of spikes per burst decreases consciously as the values of bi-parameters increase. Furthermore, by solving the system (1)–(3), the rules behind the variety of bursting in the model can be discussed.

The bursting with high frequency square-waves as Fig. 1(b) shows can be generated by the Chay–Keizer model in the purple and orange parts of the diagram, and the firing pattern of the model is plateau bursting. Moreover, the number of spikes in a series bursts is more than 35. In the red and pink parts in the figure, the shape of the bursting transitions to the tapered bursting is shown. Specifically, with the increase in time, the minimum number of spikes per burst basically remains the same, and their maximum decreases constantly. In the green parts of the figure, the shape of the bursting pattern is again conical. At this moment, their maximum goes on decreasing, and their minimum increases. The series of bursts, whose number of

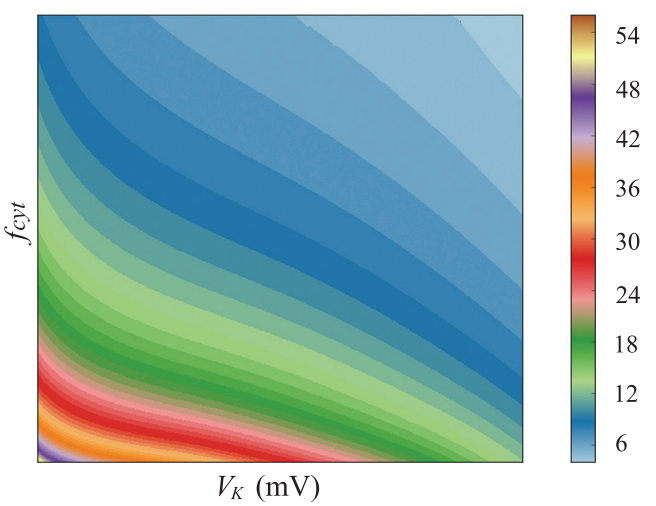

Fig. 9. Spike-counting diagram without chaos by changing values of bi-parameters. The color-coded bar in the right column shows the number of spikes within a burst. Regular bursting is expressed by the numbers 6–54.

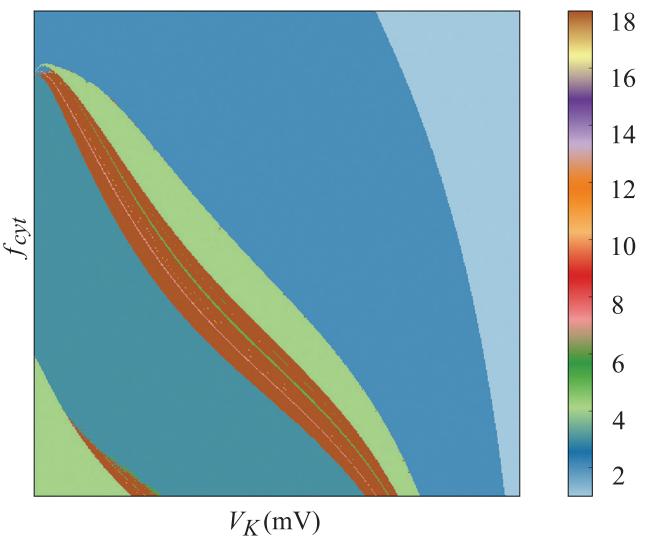

Fig. 10. Spike-counting diagram with chaos by changing values of bi-parameters. The number of spikes within a burst is also shown by the color-coded bar in the right column. The number 1 denotes tonic-spiking; the numbers 2–17 represent regular bursting, while the number 18 indicates chaotic bursting.

spikes is less than 20, keeps the square-shape around pale green parts in the diagram, and transforms to the tapered bursting eventually (blue parts). The pseudo-plateau bursting as in Fig. 1(d) is generated from the green to the blue area.

Then we keep the value range of parameter V_K, and take the value range of f_{cyt} from 0.006 to 0.12 (spike adding without chaotic region can arise between 0.003 and 0.006). The firing pattern becomes pseudo-plateau bursting. In addition, by enhancing the values of the bi-parameters, the number of spikes in one burst can change. We can clearly observe two chaotic regions in Fig. 10. And the spike adding phenomenon can occur throughout the chaotic regions which are divided into several parts by the pink and green curves which denote the periodic solutions (bursting).

4. Discussion

Based on the Chay–Keizer model, the spike adding phenomena of the mix-mode oscillation in a dynamic system are considered in this paper. An abundant variety of the bursting phenomena is observed through numerical simulations. And the rich kinetic properties of the system are discussed.

The parameters which affect the types of bursting are discussed based on the fast–slow dynamical bifurcation analysis. The process from tapered bursting to square-wave bursting is explained with the transition of the bifurcation of equilibria. Local representations of the bifurcation curves in a small neighborhood of the Bogdanov–Takens bifurcation are explored. Then the number of spikes per burst is examined. V_K is taken as the varying parameter. By analyzing the ISIs sequence, maximum and minimum of the action potential, and two types of the spike adding phenomenon — with chaos and without chaos — are explored. In addition, these results can also be obtained by changing the values of other parameters, such as f_{cyt}, v_n, and so on. Finally, the spike adding phenomenon is considered again by changing values of bi-parameters. Expressions of ISIs sequence, maximum and minimum of the action potential are provided. Analogous to the single parameter, chaotic regions are also generated for the dynamic system. Furthermore, the spike count per burst is described initially in this case. It is notable that the technique described herein can also be applied to some other biological models such as the Rose–Hindmarsh model [Ma & Feng, 2009, 2011].

Acknowledgment

This work was supported by the National Natural Science Foundation of China under Grant Nos. 11172103 and 11572127.

References

Atwater, I., Dawson, C. M., Scott, A., Eddlestone, G. & Rojas, E. [1980] "The nature of the oscillatory behavior in electrical activity for pancreatic β-cells," *Hormone Metab. Res.: Suppl. Ser.* **10**, 100–107.

Bertram, R. & Sherman, A. [2004] "A calcium-based phantom bursting model for pancreatic islets," *Bull. Math. Biol.* **66**, 1313–1344.

Carrillo, F. A., Verduzco, F. & Delgado, J. [2010] "Analysis of the Takens–Bogdanov bifurcation on m-parameterized vector fields," *Int. J. Bifurcation and Chaos* **20**, 995–1005.

Chay, T. R. & Keizer, J. [1983] "Minimal model for membrane oscillations in the pancreatic β-cell," *Biophys. J.* **42**, 181–190.

Desroches, M., Burke, J., Kaper, T. J. & Kramer, M. A. [2012] "Canards of mixed type in a neural burster," *Phys. Rev. E* **85**, 021920.

Desroches, M., Kaper, T. J. & Krupa, M. [2013] "Mixed-mode bursting oscillations: Dynamics created by a slow passage through spike-adding canard explosion in a square-wave burster," *Chaos* **23**, 046106.

Félix-Martínez, G. J. & Godínez-Fernández, J. R. [2014] "Mathematical models of electrical activity of the pancreatic β-cell: A physiological review," *Islets* **6**, e949195.

Izhikevich, E. M. [2000] "Neural excitability, spiking and bursting," *Int. J. Bifurcation and Chaos* **10**, 1171–1266.

Kinard, T. A., Vries, G., Sherman, A. & Satin, L. S. [1999] "Modulation of the bursting properties of single mouse pancreatic β-cells by artificial conductances," *Biophys. J.* **76**, 1423–1435.

Koch, C. & Segar, I. [1989] *Methods in Neuronal Modeling*: *From Synapses to Networks* (MIT Press, Cambridge, MA).

Kuznetsov, Y. A. [1998] *Elements of Applied Bifurcation Theory* (Springer-Verlag, NY).

Lang, D. A., Matthews, D. R., Burnett, M. & Turner, R. C. [1981] "Brief, irregular oscillations of basal plasma insulin and glucose concentrations in diabetic man," *Diabetes* **30**, 435–439.

Linaro, D., Champneys, A., Desroches, M. & Storace, M. [2011] "Codimension-two homoclinic bifurcations underlying spike adding in the Hindmarsh–Rose burster," *SIAM J. Appl. Dyn. Syst.* **11**, 939–962.

Lu, Q. S., Gu, H. G., Yang, Z. Q., Shi, X., Duan, L. X. & Zheng, Y. H. [2004] "Dynamics of firing patterns,

synchronization and resonances in neuronal electrical activities: Experiments and analysis," *Acta Mech. Sin.* **24**, 593–628.

Ma, S. Q. & Feng, Z. [2009] "Dynamics and double Hopf bifurcations of the Rose–Hindmarsh model with time delay," *Int. J. Bifurcation and Chaos* **19**, 3733–3751.

Ma, S. Q. & Feng, Z. [2011] "Fold-Hopf bifurcations of the Rose–Hindmarsh model with time delay," *Int. J. Bifurcation and Chaos* **21**, 437–452.

Medvedev, G. S. [2006] "Transition to bursting via deterministic chaos," *Phys. Rev. Lett.* **97**, 048102.

Meng, P., Lu, Q. S. & Wang, Q. Y. [2011] "Dynamical analysis of bursting oscillations in the Chay–Keizer model with three time scales," *Sci. China Technol. Sci.* **54**, 2024–2032.

Nowacki, J., Osinga, H. M. & Tsaneva-Atanasova, K. [2012] "Dynamical systems analysis of spike-adding mechanisms in transient bursts," *J. Math. Neurosci.* **2**, 1–28.

Osinga, H. M. & Tsaneva-Atanasova, K. [2010] "Dynamics of plateau bursting depending on the location of its equilibrium," *J. Neuroendocrinol.* **22**, 1301–1314.

Pedersen, M. G. [2009] "Contributions of mathematical modeling of beta cells to the understanding of beta-cell oscillations and insulin secretion," *J. Diabetes Sci. Technol.* **3**, 12–20.

Shilnikov, A. & Cymbalyuk, G. [2005] "Transition between tonic spiking and bursting in a neuron model via the blue-sky catastrophe," *Phys. Rev. Lett.* **94**, 048101.

Teka, W., Tsaneva-Atanasova, K., Bertram, R. & Tabak, J. [2011] "From plateau to pseudo-plateau bursting: Making the transition," *Bull. Math. Biol.* **73**, 1292–1311.

Terman, D. [1991] "Chaotic spikes arising from a model of bursting in excitable membranes," *SIAM J. Appl. Math.* **51**, 1418–1450.

Tsaneva-Atanasova, K., Osinga, H. M., Thorsten, R. & Arthur, S. [2010] "Full system bifurcation analysis of endocrine bursting models," *J. Theoret. Biol.* **264**, 1133–1146.

Vo, T., Bertram, R., Tabak, J. & Wechselberger, M. [2010] "Mixed mode oscillations as a mechanism for pseudo-plateau bursting," *J. Computat. Neurosci.* **28**, 443–458.

Vo, T., Tabak, J., Bertram, R. & Wechselberger, M. [2014] "A geometric understanding of how fast activating potassium channels promote bursting in pituitary cells," *J. Computat. Neurosci.* **36**, 259–278.

Wojcik, J. & Shilnikov, A. [2011] "Voltage interval mappings for activity transitions in neuron models for elliptic bursters," *Physica D* **240**, 1164–1180.

Yang, Z. Q. & Lu, Q. S. [2008] "Different types of bursting in Chay neuronal model," *Sci. China Ser. G: Phys. Mech. Astron.* **51**, 687–698.

Yang, Z. Q. & Guan, T. [2011] "Bifurcation analysis of complex bursting induced by two different time-scale slow variables," *Discr. Contin. Dyn. Syst.* **Supplement**, 1440–1447.

Ye, W. J., Liu, S. Q. & Liu, X. L. [2014] "Synchronization of two electrically coupled inspiratory pacemaker neurons," *Sci. China Technol. Sci.* **57**, 929–935.

Zhang, W. J., Kirk, V., Sneyd, J. & Wechselberger, M. [2011] "Changes in the criticality of Hopf bifurcations due to certain model reduction techniques in systems with multiple timescales," *J. Math. Neurosci.* **1**, 1–22.